

ISOPHOT – capabilities and performance

D. Lemke¹, U. Klaas^{1,12}, J. Abolins², P. Abraham^{1,15}, J. Acosta-Pulido^{1,3,12}, S. Bogun¹, H. Castaneda^{1,3,12}, L. Cornwall^{2,12}, L. Drury⁴, C. Gabriel¹², F. Garzón³, H.P. Gemünd⁵, U. Grözinger¹, E. Grün⁶, M. Haas¹, C. Hajduk¹, G. Hall², I. Heinrichsen^{6,12}, U. Herbstmeier¹, G. Hirth¹, R. Joseph⁷, U. Kinkel^{1,12}, S. Kirches¹, C. Kömpe⁸, W. Krätschmer⁶, E. Kreysa⁵, H. Krüger¹, M. Kunkel¹, R. Laureijs¹², P. Lützow-Wentzky¹, K. Mattila⁹, T. Müller¹, T. Pacher¹, G. Pelz^{1,12}, E. Popow¹⁰, I. Rasmussen¹¹, J. Rodríguez Espinosa³, P. Richards², S. Russell⁴, H. Schnopper¹¹, J. Schubert¹, B. Schulz¹², C. Telesco¹³, C. Tilgner¹, R. Tuffs⁶, H. Völk⁶, H. Walker², M. Wells¹⁴, and J. Wolf¹ *,**

¹ Max-Planck-Institut für Astronomie, Königstuhl 17, D-69117 Heidelberg, Germany

² Rutherford Appleton Laboratory, Chilton, Didcot, OX11 0QX, UK

³ Instituto de Astrofísica de Canarias, E-38200 La Laguna, Tenerife, Spain

⁴ Dublin Institute for Advanced Studies, School of Cosmic Physics, 5 Merrion Square, Ireland

⁵ Max-Planck-Institut für Radioastronomie, Postfach 2024, D-53010 Bonn, Germany

⁶ Max-Planck-Institut für Kernphysik, Saupfercheckweg, D-69117 Heidelberg, Germany

⁷ University of Hawaii, Institute for Astronomy, 2680 Woodlawn Drive, Honolulu, Hawaii 96822, USA

⁸ Universitäts-Sternwarte, Schillergässchen 2, D-07745 Jena, Germany

⁹ Observatory, P.O. Box 14, FIN-00014 University of Helsinki, Finland

¹⁰ Astrophysikalisches Institut Potsdam, An der Sternwarte 16, D-14482 Potsdam, Germany

¹¹ Danish Space Research Institute, Juliane Maries Vej 30, DK-2100 Copenhagen, Denmark

¹² ISO Science Operations Center, Astrophysics Division of ESA, Villafranca, Spain

¹³ Department of Astronomy, University of Florida, Gainesville, FL 32611, USA

¹⁴ University of Edinburgh, Royal Observatory, Edinburgh EH9 3HJ, Scotland

¹⁵ Konkoly Observatory of the Hungarian Academy of Sciences, P.O. Box 67, Budapest H-1525, Hungary

Received 2 August 1996 / Accepted 30 August 1996

Abstract. ISOPHOT covers the largest wavelength range on ISO from 2.5 to 240 μm . Its scientific capabilities include multi-filter and multi-aperture photometry, polarimetry, imaging and spectrophotometry. All modes can optionally include a focal plane chopper. The backbone of the photometric calibration are internal standard sources checked against celestial primary standards. The instrument is in excellent condition with all components functioning properly. There is increased detector noise due to the ionizing cosmic radiation affecting the detectability of the faintest sources. All lessons learnt from operating the instrument in space are continuously being implemented in the standard data reduction software packages available to every observer. Particular strengths of the instrument include the detectability of very cold sources, high resolution mapping and fast spectrophotometry. The far infrared serendipity sky survey performed during slews of the satellite has successfully started.

Key words: instrumentation: detectors, photometers – infrared: general

1. Introduction

ISOPHOT is an imaging photopolarimeter on board the Infrared Space Observatory. The design philosophy was to extend the capabilities of the photometric survey instrument of the pioneering sky survey satellite IRAS (Neugebauer et al, 1984) in several respects: (1) wider wavelength coverage, (2) higher spatial resolution, (3) higher sensitivity, (4) polarimetric and spectrophotometric potentials. Also the possibilities for (5) beam chopping, (6) internal photometric calibration, (7.) multi-filter and multi-aperture photometry, including (8) beam-size-effect and (9) wide-beam measurements were important design criteria. The resulting focal plane instrument for the cryo-vacuum is a sector shaped box which is shown in fig. 1. It is compactly filled with precisely aligned moving components such as filter wheels and chopper, a challenge for a space engineer to build and a nightmare to get accepted for flight (Lemke et al, 1993). All the detectors are bulk-type photoconductors made from three

Send offprint requests to: D. Lemke, lemke@mpia-hd.mpg.de

* several co-authors have changed the above given affiliation since their involvement in ISO

** ISO is an ESA project with instruments funded by ESA Member States (especially the PI countries: France, Germany, the Netherlands and the United Kingdom) and with the participation of ISAS and NASA.

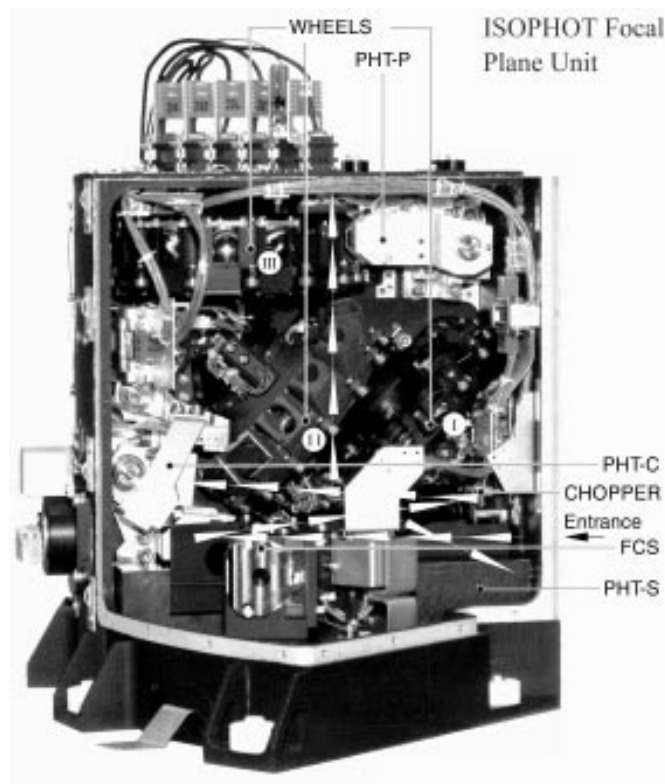


Fig. 1. The ISOPHOT focal plane unit has a height of 25 cm. The beam from the telescope, after deflection by the pyramid mirror, enters from the right (arrow) and is deflected by an imaging mirror (left) to the chopper mirror (right). Distribution to the several subinstruments is via optical elements on wheel I.

extrinsic materials: Si:Ga, Si:B, stressed and unstressed Ge:Ga. The other initially foreseen materials, InSb and Si:P, behaved less favorably under ISO's low background and low temperature conditions and were after all not included.

ISOPHOT houses several subsystems: a multi-filter multi-aperture photopolarimeter (PHT-P), two far infrared cameras (PHT-C), a spectrophotometer for the near and mid infrared (PHT-S), 4 internal calibration sources (two thermal radiation sources (TRS) form 2 redundant fine calibration sources (FCS)) and a focal plane chopper.

The instrument is operated via Astronomical Observing Templates (AOTs), electronic questionnaires to be filled in by the user with source and observing parameters. The AOT aided observations are electronically processed for satellite commanding, the astronomical data obtained are automatically fed into pipeline data processing. There are 9 observing modes which can be grouped into (i) multifilter photometry, (ii) absolute photometry, (iii) multiaperture photometry, (iv) sparse maps (scattered sources in a 3° field), (v) mapping and scanning and (vi) spectrophotometry. Polarization measurements use AOTs which are not automatically performed but need intervention by experts via the Calibration Uplink Language. Detailed descriptions and complementing user information can be found in Lemke et al (1993), (1994), Grözinger et al (1993), Gemünd et

al (1994) and in the ISOPHOT Observer's Manual, Klaas et al (1994).

2. Preflight Calibration

The goals of the preflight calibration were (1) to demonstrate that the instrument would maintain a photometric calibration over a period of several months, (2) to set all operational parameters (detector bias voltages, temperatures, ...) to optimal values in the incident and background flux range expected in orbit and (3) to vary all operational parameters also to their extreme values, in order to gain experience with the operation and to be prepared for any unexpected behaviour in orbit.

The calibration was done on three levels. All detectors, filters, lenses, mirrors, gratings and polarizers were measured at cryotemperature for their relevant wavelength-dependent sensitivity, transmission, reflectivity and polarization. Next, the subsystems (like the spectrophotometer PHT-S) were calibrated again at cryotemperatures and the result checked for consistency with predictions based on the above component tests. Finally, the completed ISOPHOT instrument was calibrated in a specially designed calibration chamber simulating the operational temperature (1.8...3.4 K), the low background flux ($< 10^8 \text{ ph s}^{-1} \text{ cm}^{-2}$) and the telescope beam ($f/15$) of the ISO satellite (Wolf et al, 1994). A chopped warm black body (300..500..900K) was used as calibration source. The low background was generated by cold exchangeable neutral density filters with transmissions of $10^{-4} \dots 10^{-9}$. The fourth step, calibrating the instrument integrated into the satellite together with ISO's telescope was not foreseen. Functional checks with the cold satellite prior to launch demonstrated excellent functioning of all components, but the photometric performance was partially affected by thermal leaks in the cryo-cover of the satellite.

The results of the instrument level calibration are summarized in tab. 1. They were the basis for the prediction of the ultimate performance in flight on a "dark" sky, as given in the Observer's Manual. Degradations to be expected in flight due to the real and structured sky (galaxies, cirrus), detector drifts and cosmic particle hits were not included in the NEPs measured in the laboratory.

3. Preflight preparation for high energy radiation effects and their curing

Exposing the detectors to ionizing radiation results in (1) spiking, (2) increase in responsivity and (3) an even faster increase of noise. In order to simulate the daily passage of the satellite through the earth's radiation belts, all detectors were exposed in a laboratory cryostat to Gamma-radiation of a radioactive ^{137}Cs source (0.662 MeV). The dose of 3.7 rad, equivalent to one passage through the Van Allen belt, resulted in a responsivity increase of $\lesssim 10\%$ for the Si:X detectors and $\gtrsim 100\%$ for the Ge:X sensors. This is caused by recharging of all impurity centers in the crystal when flooded with electrical carriers generated by the ionizing bremsstrahlung and fast electrons, thereby increasing the lifetime of IR generated carriers (Petroff,

Table 1. Characteristics of the ISOPHOT photodetectors measured in the preflight calibration and the present minimal detectable flux inflight. The latter numbers are given for a $S/N = 1$ and an integration time on point sources of 256 seconds. The values given here were measured at the sky background given in the last column at 11μ for P1, at 25μ for P2, at $60 \mu\text{m}$ for P3, at $90 \mu\text{m}$ for C100 and $175 \mu\text{m}$ for C200. The minimal detectable flux depends somewhat on the observing technique used and is limited by the accuracy of sky background subtraction, flat fielding, spike history and the time elapsed since last curing. With improving correction techniques these values will decrease.

Detector	Material	Peak Response [μm]	T [K]	Bias [V]	Responsivity [A/W] preflight	Dark current [e/s] preflight	Dark current [e/s] in-flight	NEP [$\text{W}/\sqrt{\text{Hz}}$] preflight	Minim. detect. flux [mJy] in-flight	Sky Background [MJy sr^{-1}]
P1	Si:Ga	15	2.9	90	0.6	1595	1460	$1.6 \cdot 10^{-16}$	5	15
P2	Si:B	25	3.6	10	0.7	3825	5960	$2.2 \cdot 10^{-16}$	13	40
P3	Ge:Ga	100	2.8	0.25	17	123	19700	$3.5 \cdot 10^{-18}$	20	10
C100	Ge:Ga	100	3.0	0.18	29	7471	25000	$8.7 \cdot 10^{-18}$	5..10	7
C200	Ge:Ga str.	180	1.8	0.08	15	1869	4000	$1.2 \cdot 10^{-17}$	45	7
S1 (SL)	Si:Ga	15	2.9	37	1.3	< 500	< 500	$2.1 \cdot 10^{-17}$	10	15
S2 (SS)	Si:Ga	15	3.0	37	3.9	< 500	< 500	$1.0 \cdot 10^{-17}$	26	0.5

1979). It takes hours for the increased responsivity and noise to shrink spontaneously to the original values. Therefore curing methods had to be developed to reestablish the responsivity (= calibration) faster. Given the tough limits of heat dissipation in the instrument, three methods are available: (1) bias boost, (2) temperature increase to $T < 19 \text{ K}$, (3) flashing with infrared radiation by the internal calibrators ($< 10^{-9} \text{ W / pixel}$). Best results were achieved by a combination of these methods as described by Blum et al (1990), Schiessl et al (1991) and Schubert, Roth et al (1995). The original calibration could be reestablished within 10 minutes to within 5% of its original value. The radiation effects caused by heavier charged particles, such as protons, which are also present in the cosmic radiation outside the belts, were not studied for schedule reasons.

Potential proton radiation damage to optical components such as filters, field lenses, blockers made of quartz, anorganic crystals and plastics were also studied at cryogenic temperature. A total dose of a factor 60 higher than the full mission dose of 4 Krad (SI) was applied to the cold components using an alpha-radiating ^{241}Am source. Only the transmission curves of organic components used as antireflection coatings were slightly affected by this irradiation (Schubert, Lemke et al, 1994).

4. Inflight Commissioning

All parts of the instrument were found to work in space like on earth. In particular, the filter wheels and the chopper act on telecommands with high precision and low power dissipation. The laboratory curing procedures developed for the temporary radiation damage in the detectors caused in the earth's radiation belts had only to be modified slightly (Tab. 2). Three hours after perigee passage a curing sequence is started which, within 45 minutes, heals all detector units of ISOPHOT. The responsivity level achieved by this standard curing sequence varies slightly from day to day and seems to depend on the solar activity. The

Table 2. Curing of the high energy radiation induced responsivity (R) increase after passage through the earth radiation belts. Procedures for Si:B (P2) and Ge:Ga (C100) are given as examples. Curing is performed by changing the temperature T, the bias V_b and irradiating the sensor with IR photons. C100 is flashed a second time 12 minutes after the first flash.

Detector	R increase	T [K]	V_b [V]	IR flash [W/pixel], duration [s]
P2	$\sim 10\%$	$3.6 \Rightarrow 19$	-	-
C100	$\sim 50\%$	3.0	$-0.18 \Rightarrow -0.22$ -0.18	$5 \cdot 10^{-11}$, 128 $5 \cdot 10^{-11}$, 256

Cosmic Radiation outside the belts leads to a slow increase of the responsivity (fig. 2) along the orbit and also causes occasional large spikes (fig. 3) and continuous low level noise. While spikes producing voltage steps smaller than 40 mV on the integration ramps are difficult to distinguish from the detector / preamp noise, about 0.5 spikes per second and per mm^3 detector volume are counted on average above this noise level.

The only deviations from the almost perfect and expected behaviour are:

- A sudden flux change of one of the internal calibrators (TRS2, FCS1) by about a factor of two on orbit 94. The likely reason is a flake off from the heater caused by the continual thermal stress. This required recalibration of the TRS and calibration of the redundant TRS.

- A greater vulnerability of the P3 sensor (Ge:Ga) to ionizing radiation. Its responsivity can increase by a factor of two within 7 hours (and the noise even faster) in the "quiet" cosmic environment outside the belts.

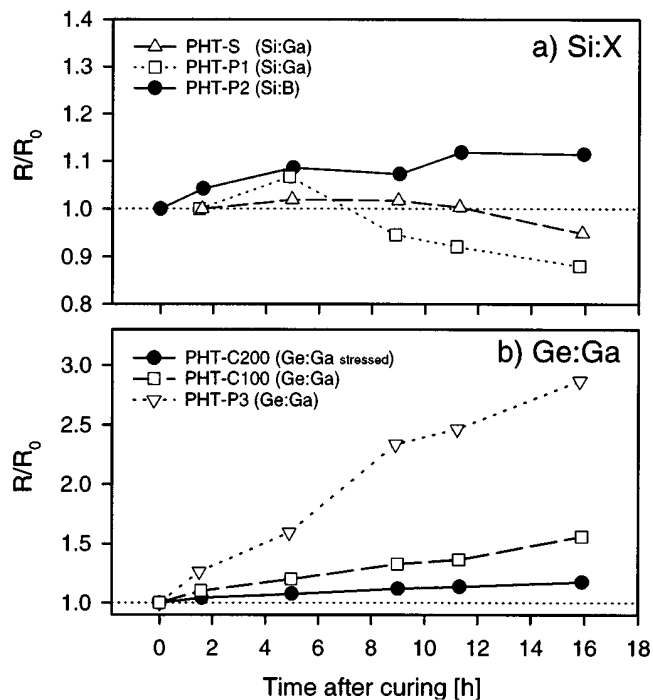


Fig. 2. The slow responsivity (R) increase of detectors caused by cosmic ray particle hits during the 16 hour science window on orbit no. 21. After passage of the radiation belts the detectors are cured to their nominal responsivity R_0 . Values of PHT-S and P1 start at ~ 2 h, because initially they are disturbed by memory effects caused by heating, flashing and bias change.

- A slow signal drift for many seconds after large ionizing particle hits, which increases the detection limit for the faintest sources (Fig. 3).

- Occasional "latch-up" effects in the cold-read-out electronics (CRE) of the P2 sensor required repetition of some measurements. A prevention procedure is currently being developed in the laboratory.

- While all other AOTs have been commissioned successfully, the absolute photometry modes (AOTs 05, 25) required additional options to be included in order to measure the ionizing radiation induced dark current changes and suspected straylight.

Pleasant surprises were (1) the high speed of spectrophotometric measurements using PHT-S for surveys of larger samples of objects, (2) the capability for fast high resolution mapping involving chopping and satellite rastering by applying the Astronomical Observing Template P32 and (3) the detectability of very cold sources. Examples of results are given elsewhere in this issue (Gürtler et al (1996), Hippelein et al (1996), Laureijs et al (1996), Walker et al (1996)). Also the ISOPHOT Serendipity Sky Survey has been commissioned successfully after the broad $175 \mu\text{m}$ filter was selected following comparative test observation with other FIR filters. This project is described in a separate letter in this issue (Bogun et al 1996).

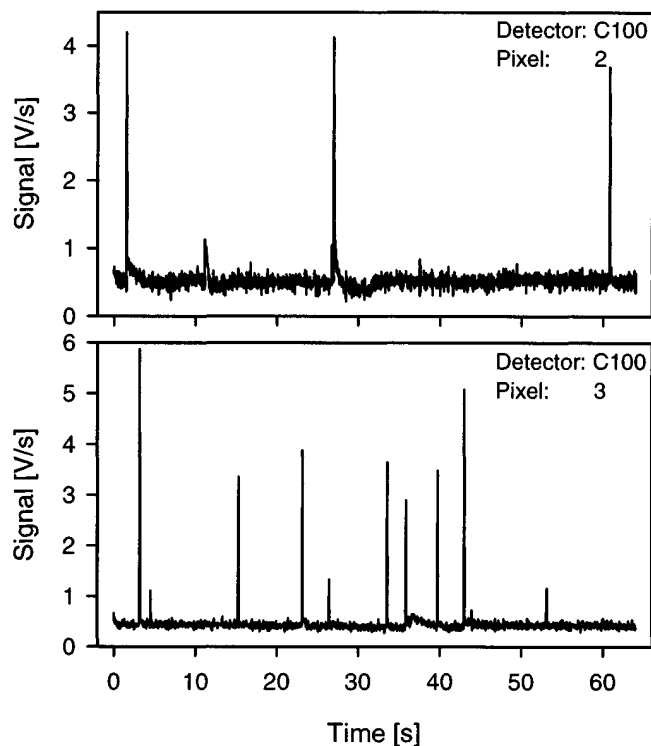


Fig. 3. Cosmic particle hits as seen by pixel 2 and 3 of the C100 camera during a 64 s integration. They cause spikes and drifts of the small signal level.

5. Inflight Calibration

5.1. PHT-P and PHT-C

This is done by celestial standards: stars, planets and asteroids. They are used to calibrate the internal standards (FCS). Every observation is then checked against a short illumination by the FCS. The FCS power is tuned according to the observers flux prediction to deliver a signal similar to the celestial target. That avoids detector drifts caused by large flux steps. In practice this method has to overcome several difficulties:

- The continuous responsivity increase of the Ge:Ga detectors in particular along the orbit. This requires a continuous recalibration because the signal of the celestial target depends on the position along the orbit. Therefore interpolations and extrapolations towards actual responsivity values are necessary. Furthermore, every calibration flash acts as a partial recurring. A definite recurring of the detectors near apogee now reduces this complication.

- The integration ramps of the Ge:Ga and the stressed Ge:Ga detectors are not linear. This is a property of the cold read-out electronics (CRE), an integrating amplifier, which effectively reduces the bias voltage on the detector by ~ 40 mV, if the capacitor is charged to its maximum of 2 V. This "debiasing" effect is strongest on the C200 camera with a bias voltage of 80 mV (fig. 4). Software has been developed to correct for this and some intrinsic nonlinearities of this newly developed circuit, the latter being also present in the other detector channels.

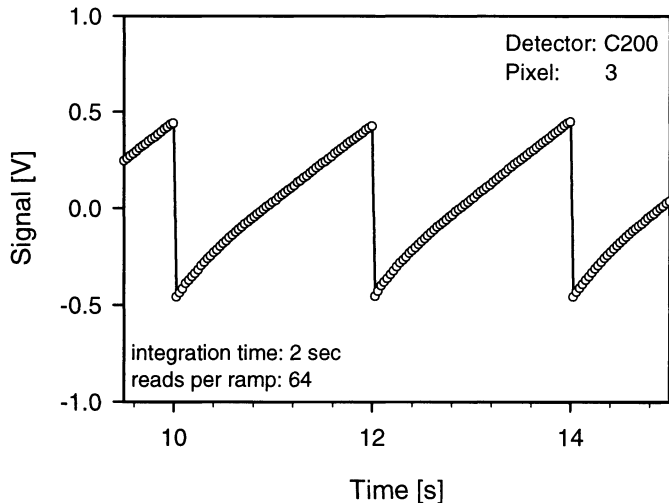


Fig. 4. The integration ramp of one C200 camera pixel is not straight because of small non-linearities in the cold read-out electronics and because of "debiasing" of the detector with increasing charging of the integrating capacitor. C200 with a bias voltage of only 80 mV suffers from this debiasing, which is corrected for in the data evaluation. This effect is negligible for most other detectors.

- The signal drifts for some time after an illumination change. At very low fluxes it takes minutes before 95% of the final signal is met. Model drift curves for all detectors developed by Schubert et al (1995) should correct for this effect in the future.

- Although tightly baffled sky straylight is present in faint object detections. Its exact amount will be measured soon in a dedicated program.

Stars are used as celestial standards for the near and middle infrared. They also serve as faint standards (<100 mJy) in the far infrared (Cohen et al, 1995 and Hammersley, 1995). In addition asteroids are used for wavelengths up to $200 \mu\text{m}$; however corrections for light curve, distance and phase angle have to be applied. They are calibrated against Mars and Uranus in a preparatory program using the Kuiper Airborne Observatory (Telesco 1994). Applying the Standard Thermal Model (Lebofsky et al 1986) their FIR fluxes can be predicted to $\pm 30\%$. Light curve corrections from ongoing ground observing programs and improved thermal models will soon improve this accuracy to better than $\pm 20\%$. While the FIR flux of the asteroids used (Ceres, Herculina, Chaldaea, ...) is about 100 Jy, Uranus and Neptune with their tenfold larger fluxes are also used for cross-calibration with other instruments.

The exact photometric calibration of ISOPHOT is a major task, given its large number of modes and the disturbances caused by the cosmic radiation. It will continuously be improved during the mission. At present the error budget contains (1) the uncertainties of the celestial standards of about $<10\%$ for stars, $\sim 20\%$ for asteroids, (2) color corrections for target spectra different from the calibrator ($\sim 10\%$), (3) instrumental effects such as uncertainties of beam profiles, straylight, potential filter leaks ($\sim 10\%$), (4) detector effects such as photon noise, read-noise,

non-linearities, transients, spikes, all of which are variable and (5) sky background uncertainties caused by cirrus, galaxies, insufficient flat fielding and pointing errors. The photometric accuracy improves with decreasing wavelengths and increasing brightness of the sources. It is estimated to be $<20\%$ in the middle IR ($\lambda \lesssim 30 \mu\text{m}$) for sources brighter than 1 Jy. For faint sources the error components (4) and (5) dominate at all wavelengths (see section 6). For the far infrared $\lambda \gtrsim 50 \mu\text{m}$ it now seems feasible to achieve soon an absolute photometric accuracy of better than $\pm 30\%$. Recalibrations planned for post mission will improve these values. The most up to date calibration files are continually applied to all data products and are available from the ISOPHOT Data Center at MPIA Heidelberg.

5.2. PHT-S

The internal source FCS is not used with the spectrophotometer because it requires the FCS to be heated to 250 K to produce a detectable signal at the short end ($2.5 \mu\text{m}$), which would result in saturation of the $\sim 10 \mu\text{m}$ pixels and cause a memory effect. Therefore stars (HR 6705, HR 6688) are used as calibrators. The resulting spectral response function of the spectrophotometer is plotted in fig. 5. While the shape of this curve is well established, the absolute response values depend on the position of a pointlike source in the aperture: for offsets of ± 6 arc sec from the maximum (<3 arc sec off the center of the aperture and wavelength dependent) the signal can be attenuated by $<30\%$. For extended source measurements corrections with the wavelength dependent beam profiles have to be applied. The pixels at $\lambda \lesssim 3 \mu\text{m}$ suffer more from drift effects than the rest of the arrays. The dark current is individual for each pixel; standard values based on the weekly routine calibration can be used for the data reduction. The wavelength calibration was performed on atomic and ionic lines of Planetary Nebulae. The error in this calibration is $\pm 0.003 \mu\text{m}$ for the center of the short wavelength array and increases to $\pm 0.007 \mu\text{m}$ towards its edges; $\pm 0.006 \mu\text{m}$ at the center and $\pm 0.018 \mu\text{m}$ are the respective uncertainties for the long wavelength array. Cross-calibration with other spectrometers on ISO demonstrates good agreement (Kessler et al 1996).

6. Sensitivity limits

The dark current increase in the FIR due to ionizing radiation and as compared to ground tests of the detectors ranges from a factor <1.1 (P1, -S) to a factor 2 (P2, C200) and a factor 3 (C100). An exception is P3 which was excellent on ground ($<130 \text{ e s}^{-1}$) and is now up by 2 orders of magnitude resulting in a NEP increase to $5.6 \cdot 10^{-17} \text{ W Hz}^{-\frac{1}{2}}$.

Using faint stars of Cohen (1996) with fluxes of 70 mJy at $90 \mu\text{m}$ and carefully correcting for dark current and sky straylight we obtained detection limits of 5 to 10 mJy at $90 \mu\text{m}$ for $S/N \sim 1$ and 256 seconds integration time on source (Tab. 1). The corresponding preliminary limit at $175 \mu\text{m}$ is 45 mJy. These values are achieved at sky background levels of 7 MJy sr^{-1} and are limited by the accuracy of background subtraction

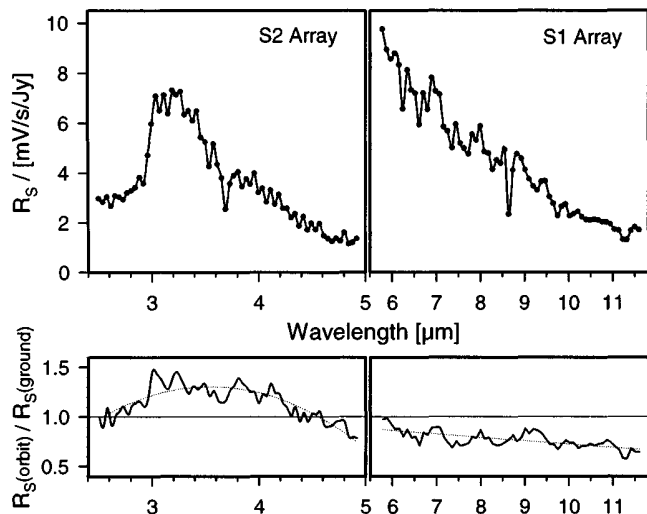


Fig. 5. Top: The spectral response function R_s for the spectrophotometer PHT-S connects the signal strength [mV/s] with the flux [Jy] of the celestial target. Bright stellar continua were used for this calibration. The central pixel of both arrays is at the edge of the order sorting filters. Below: Comparison of the spectral response functions measured preflight and during the mission.

and the present accuracy of the flat fielding (<2%) of C100 and C200 where individual pixels have different drift and memory characteristics. Different techniques may be considered for faint source detection depending also on the characteristics of the background environment: (1) triangular chopping (at low source / background contrast), (2) mapping (at complex background structures) or (3) staring (for several nearby sources saving extra background measurements). Investigations made so far have shown only minor differences when these techniques were tested on faint stars.

7. Data Evaluation

The data reduction can be performed with dedicated program tools: The pipeline software provides a standard reduction adapted for each AOT. The PHT interactive analysis (PIA) tool allows a more detailed look at intermediate steps and improvement of the results individually. This data reduction includes the following steps: corrections for nonlinearity of signal integration ramps, for cosmic radiation events and (soon) for detector transient drifts, determination of the signal (per ramp and per chopper plateau), determination of the detector responsivity and flux calibration. It can also be applied to the calibration of sky background measurements, multi-filter and multi-aperture photometry and mapping. The data reduction steps and their products are described in the ISOPHOT Data Users Manual (Laureijs et al, 1996) and in the ISOPHOT Interactive Analysis Users Manual (Gabriel et al, 1996).

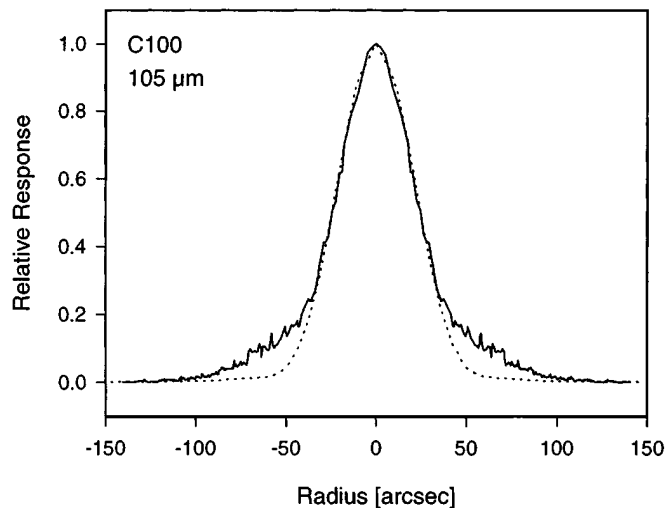


Fig. 6. The average beam profile (solid line) of the C100 pixels at $\lambda = 105 \mu\text{m}$. They were measured on a pointlike source (NGC 6543) with 15 arc sec stepwidth. The dotted line represents the theoretical profile for the convolution of the square pixel with the Airy function.

8. Next Steps

The following upgrades to the calibration, which will become generally available through calibration files contained on all data deliveries (CDs) and by updated deliveries of the data evaluation packages (section 7), are in preparation:

1. Implementation of standard detector drift curves.
2. More accurate beam profiles (example in fig. 6).
3. Straylight corrections.

The internal calibrators FCS will be updated continuously by weekly checks on celestial standards. Corrections for long term drifts (if there are any) will be implemented into the calibration files. Measurements of the instrumental polarization degree and angle have only just started. The polarization degree is typically 10%, as was expected from ground tests without the telescope. These results will be published later.

Acknowledgements. ISOPHOT was funded by the Deutsche Agentur für Raumfahrtangelegenheiten DARA, the Max-Planck Society, the Danish, British and Spanish Space Agencies and several European and American institutes. We thank the industrial contractors Dornier, Zeiss, Battelle, Imec and Casa for excellent work and the European Space Agency for success orientated collaboration. Erick Young, Tucson, contributed to the selection of the P2 detector pixels. We acknowledge the continuous support of S. Beckwith and H. Elsässer at MPIA in Heidelberg, where with their help we were able to set up a dedicated ISOPHOT Data Center.

References

- Blum, J., Hajduk, C., Lemke, D., Salama, A., Wolf, J. 1990, High-energy radiation effects on the ISOPHOT far-infrared detectors, *Infrared Phys.*, 30, 93-96
- Bogun, S., Lemke, D., Klaas, U., Herbstmeier, U., Assendorp, R., Richter, G., Laureijs, R., Kessler, M.F., Burgdorf, M., Schulz, B., Pelz, G., Beichman, C.A., Rowan-Robinson, M. 1996, First de-

- tections of the ISOPHOT FIR Serendipity Survey, *Astronomy and Astrophysics*, this issue
- Cohen, M., Witteborn, F.C., Carbon, D.F., Davies, J.K., Wooden, D.H. Bragman, J.D. 1996, *AJ*, in press
- Cohen, M., Witteborn, F.C., Walker, R.J., Bragman, J.D., Wooden, D.H. 1995, Spectral Irradiance Calibration in the Infrared. IV. 1.2 to 35 μm spectra of 6 standard stars, *AJ* 110, 275
- Gabriel, C., Haas, M., Heinrichsen, I., Tai, W.-M. 1996, ISOPHOT Interactive Analysis Users Manual, available from ESA/ISO Ground Observatory VILSPA or MPI Astronomie Heidelberg
- Gemünd, H.P., Kreysa, E., Schubert, J., Krätschmer, W. 1994, High-Performance FIR-Bandpass Filters for the ISOPHOT Instrument, *Proc. SPIE* 2268, 272-282
- Grözinger, U., Kirches, S., Lemke, D., Schubert, J., Schulz, B., Wolf, J. 1993, Characterisation of the detectors and calibration of the ISOPHOT experiment, *Proc. Photon Detectors for Space Instr.*, ESA SP-356, 329
- Gürtler et al 1996, Detection of solid CO₂ towards young stellar objects, this issue
- Hammersley, P. 1995, private communication
- Kessler, M. et al 1996, this issue
- Klaas, U., Krüger, H., Heinrichsen, I., Heske, A., Laureijs, R. (eds) 1994, ISOPHOT Observer's Manual, version 3.1
- Hippelein et al 1996, Far Infrared Mapping of the Galaxies M 51 and M 101 with ISOPHOT, this issue
- Laureijs, R.J. et al 1996, Very small grain emission in NGC 7023, this issue
- Laureijs, R.J., Richards, P.J., Krüger, H. 1996, ISOPHOT Data Users Manual", V2.0, 1996, available from ESA/ISO Ground Observatory VILSPA or MPI Astronomie Heidelberg
- Lebofsky, L. et al, 1986, *Icarus* 68, 239
- Lemke, D., Garzon, F., Gemünd, H.P., Grözinger, U., Heinrichsen, I., Klaas, U., Krätschmer, W., Kreysa, E., Lützw-Wentzky, P., Schubert, J., Wells, M., Wolf, J. 1994, Far-infrared imaging, polarimetry and spectrometry on the Infrared Space Observatory, *Opt. Eng.* 33(1), 20
- Lemke, D., Lützw-Wentzky, P., Fricke, W., Bollinger, W. 1993, Cryogenic Aspects of ISOPHOT, the Photometer for the ISO Satellite, *Cryogenics*, 33, 395
- Lemke, D., Wolf, J., Schubert, J., Patrashin, M. 1993, ISOPHOT - the imaging photopolarimeter for the Infrared Space Observatory, *Proc. SPIE* 1946, 261
- Neugebauer et al 1984, *ApJ* 278,L1
- Petroff, M.D., Pickel, J.C., Curry, M.P. 1979, Low-level radiation effects in extrinsic infrared detectors, *IEEE Transactions on Nuclear Science*, NS-26, 4840
- Schiessl, U., Tacke, M., Wolf, J., Lemke, D. 1991, Annealing of infrared photoconductors with infrared diode lasers, *Experimental Astron.*, 2, 139
- Schubert, J., Fouks, B.I., Lemke, D., Wolf, J. 1995, Transient Response of ISOPHOT Si:Ga Infrared Photodetectors: Experimental Results and Application of the Theory of Nonstationary Processes, *SPIE* 2553, 461
- Schubert, J., Lemke, D., Krätschmer, W., Mampel, K. 1995, α -Radiation Tests on the Transmission of Cryogenically Cooled Infrared Filter Materials used in ISOPHOT, *Proc. SPIE* 2553, 288
- Schubert, J., Roth, G., Wolf, J., Lemke, D. 1994, Correction and curing of in-orbit induced non-ideal behaviours of ISOPHOT's photodetectors, *Proc. SPIE* 2268, 283-294
- Telesco, C. 1994, private communication
- Tuffs et al 1996, ISOPHOT Maps of NGC 6946 in the range λ 50 - 240 μm , this issue
- Walker et al 1996, ISOPHOT observations of R CrB: a star caught smoking, this issue
- Wolf, J., Gabriel, C., Grözinger, U., Heinrichsen, I., Hirth, G., Kirches, S., Lemke, D., Schubert, J., Schulz, B., Tilgner, C., Boison, M., Frey, A., Rasmussen, I., Wagner, R., Proetel, K. 1994, Calibration facility and the preflight characterization of the photometer in the Infrared Space Observatory, *Opt. Eng.*, 33, 26, also published in *Proc. SPIE* 2019, 82